Pergamon

Int. J. Heat Mass Transfer. Vol. 40, No. 1, pp. 39–48, 1997

0017–9310/97 $15.00+0.00

PII: S0017–9310(96)00090–7

Enhancement of heat transfer using porous convection-to-radiation converter for laminar flow in a circular duct

J. M. ZHANG, W. H. SUTTON and F. C. LAI†

School of Aerospace and Mechanical Engineering, University of Oklahoma, Norman, OK 73019, U.S.A.

(*Received* 7 *November* 1995 *and in final form* 15 *February* 1996)

Abstract—The convection-to-radiation converter (CRC) made of porous ceramics has been proven to be an effective means in the enhancement of heat transfer in burners, combustors, industrial furnaces and high temperature plug flow systems. The paper proposes a novel application using this CRC technique in a partial bypass flow system for potential heat transfer enhancement. Hydrodynamically fully-developed and thermally developing laminar flow is assumed in a circular duct which is fitted with a porous core to enhance both convective and radiative transfer from a high-temperature gaseous medium to a heat-absorbing wall. The Navier–Stokes and modified Darcy equations are applied, respectively, to the flow field in a gas layer and porous core region. The radiation field is modeled by a two-dimensional S-type integral equation of transfer for its accuracy and efficiency in the numerical calculations. The effects of heat transfer augmentation using a porous CRC are investigated numerically for various flow and thermal parameters. Numerical solutions which include velocity profiles and flow characteristics of the CRC system as well as isotherm patterns, parameterization of the heat fluxes, mean bulk temperature and Nusselt number distributions along the flow direction are presented. Copyright © 1996 Elsevier Science Ltd.

1. INTRODUCTION

Techniques for the enhancement of combined radiative and convective heat transfer have become increasingly important during the last two decades in developing compact and efficient high-temperature thermal energy systems. Applications include industrial furnaces, heat exchangers, combustors and thermal energy storage devices, where the convection and radiation modes of heat transfer are both important. One of the promising techniques is to use porous materials to increase heat transfer by convective–radiative exchange due to a significantly large surface area of the porous medium. This technique has been applied to various industrial furnaces and combustor–incinerators, and remarkable energy savings and heat transfer enhancement have been demonstrated [1–6].

From the beginning of the 1980s, Echigo [1, 3, 4] has successfully developed techniques using a foam ceramic and metal matrix porous structure, which has been termed as a convection-to-radiation converter (CRC), to enhance heat transfer and recover heat from exhaust gas in industrial furnaces and combustion systems. As indicated by Echigo [1], the heat transfer enhancement in a high-temperature plug flow channel with a porous segment placed normal to the flow direction is mainly due to two effects: one is the radiation shield effect of the porous medium, the second is the effective combined convection–radiation heat transfer process, i.e. the convective heat transfer on the gas–solid interface to raise the temperature of the porous medium and then the conversion of thermal energy in the porous medium to radiation. Since the porous materials have a very large surface area per unit volume and usually possess a much stronger thermal radiation emittance than gas media, the radiative flux emitted by the porous insert at high temperature is much larger than that emitted by the gaseous fluid. In addition, the temperature of the gas–solid medium decreases sharply along the flow direction, the thermal radiation emitted by the porous medium propagates mainly back in the upstream direction. This makes the upstream side a strong thermal radiation field and the downstream a weak radiation area for the plug flow. The numerical analysis of heat transfer from a plug flow in a rectangular channel has been performed by Echigo [1] based on the assumptions that the gas is nonradiating and the scattering effect in a porous medium is negligible. It is found that a drastic temperature drop (more than 300 K) in the flowing gas can be achieved within a very short distance (on the order of 1 cm) due to the strong directionality of the convection–radiation converter. Wang and Tien [7] presented a two-flux gray radiation model which includes the scattering property of the porous medium by direct application of the electromagnetic Mie theory. Their numerical results indicate that both the scattering albedo and back-scattering fraction factor play an important role in the heat transfer per-

† Author to whom correspondence should be addressed.

NOMENCLATURE

c_p	specific heat at constant pressure
d	distance
F	function of inertial terms
G	incident radiation
h	dimensionless characteristic pore size
I	radiation intensity
k	conductivity
K	permeability of the porous medium
L	length of the circular duct
$\dot{m}$	mass flow
Nu	modified Nusselt number
n	reflection index
p	pressure
Pe	Peclet number
Pr	Prandtl number
q	heat flux
R	radius of the circular duct
Re	Reynolds number
r	radius
S	radiative source function
s	distance from boundary to a point in the medium along a ray of intensity
T	temperature
u	velocity
x	segment of traveling length of a radiation ray
z	axial length.

Greek symbols

β	extinction coefficient
δ	porosity of the porous medium
ε	wall emissivity
ϕ	azimuth angle
Φ	nondimensional divergence of radiative flux
γ	ratio of conductivity
Γ	inertial coefficient
η	nondimensional axial distance
Λ	ratio of pressure gradient
μ	dynamic viscosity
ν	kinematic viscosity
N	conduction–radiation parameter
θ	nondimensional temperature
ρ	density
σ	Stefan–Boltzman constant
τ	optical thickness
ω	single scattering albedo
ξ	nondimensional radius.

Superscript

*	nondimensional quantity.

Subscripts

0	inlet condition
C	convection
f	fluid
i	interface
m	mean value
p	porous medium
R	radiation.

formance. The effect of gaseous radiation was investigated by Echigo *et al.* [8], and the transient heat transfer response (simultaneous conduction, convection and radiation) was analyzed theoretically and experimentally in the subsequent work [9]. However, it should be pointed out that the analyses performed in the previous studies were mostly based on the one-dimensional assumption or simplification. For low temperature applications (i.e. negligible radiation heat transfer), the enhancement in heat transfer using porous inserts has been considered by Tong *et al.* [10].

Since the porous materials of large permeability possess a large surface area per unit volume and a radiative extinction coefficient on the order of 100 m^{-1}, it is expected that the insertion of a porous core in the flow system in Fig. 1 can effectively improve the heat transfer performance due to its combined convection–radiation effects. For a complete understanding of the combined heat transfer process in the proposed system, numerical investigations are performed for various flows and thermal conditions. The Navier–Stokes and modified Darcy equations are applied to the flow in the fluid layer and porous core, respectively. The newly developed S-type integral equation of radiative transfer [11] is used to predict radiation in the two-dimensional nonhomogeneous participating medium. An iterative scheme is employed to solve the highly nonlinear system of equations. The results of the heat transfer augmentation are presented for a wide range of parameters.

2. FORMULATION OF THE PROBLEM

For the flow system shown in Fig. 1, a steady, incompressible, hydrodynamically fully-developed laminar flow is assumed. The working fluid, a radiative gas medium, enters the duct with a uniform temperature T_0 and is cooled by the heat-absorbing wall at constant temperature T_w. The porous core is assumed to have a foam-type structure and thus has a very high permeability. For radiation transport, the whole flow region including the porous core is considered as a gray, nonhomogeneous participating medium.

Momentum and energy equations

Since the flow is assumed to be hydrodynamically fully-developed and thermally developing, the equa-

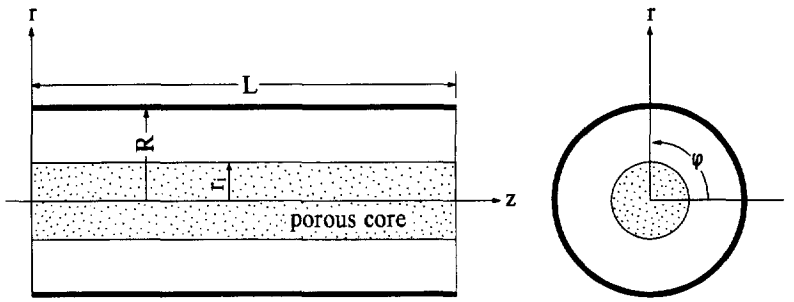

Fig. 1. A schematic of the flow system and coordinates.

tions governing the velocity and temperature fields in the gas layer can be written as

$$\frac{dp}{dz} = \mu \frac{1}{r}\frac{d}{dr}\left(r\frac{du}{dr}\right) \tag{1}$$

and

$$\rho c_p u \frac{\partial T}{\partial z} = k_f\left[\frac{1}{r}\frac{\partial}{\partial r}\left(r\frac{\partial T}{\partial r}\right)+\frac{\partial^2 T}{\partial z^2}\right]-\nabla\cdot\mathbf{q}_R \tag{2}$$

where $\mathbf{q}_R$ is the net radiative heat flux because the medium is considered to be radiatively participating.

Further, it is assumed that local thermal equilibrium is established in the porous core, and the inertial effects are important because of the high permeability and high local velocity involved. The modified Darcy and energy equations are applied to this flow region, which are given by

$$\frac{dp}{dz} = -\left(\frac{\mu}{K}+\frac{\rho\delta F}{\sqrt{K}}u\right)u+\mu_e\frac{1}{r}\frac{d}{dr}\left(r\frac{du}{dr}\right) \tag{3}$$

and

$$\rho c_p u \frac{\partial T}{\partial z} = k_e\left[\frac{1}{r}\frac{\partial}{\partial r}\left(r\frac{\partial T}{\partial r}\right)+\frac{\partial^2 T}{\partial z^2}\right]-\nabla\cdot\mathbf{q}_R. \tag{4}$$

It should be noted that the second term on the right side of equation (3) represents the inertial term and the third term is the viscous term. These two terms represent the higher order correction to the Darcy's law. Strictly speaking, the effective viscosity μ_e involved in the viscous term is different from the fluid viscosity μ. However, due to the lack of definitive information on μ_e, it is customarily assumed that it has the same value as the fluid viscosity. The effective conductivity k_e is the conductivity of the porous medium, including the fluid which saturates the porous medium, and can be estimated using the mixture rule,

$$k_e = \delta k_f + (1-\delta)k_p. \tag{5}$$

The divergence of radiative heat flux for the whole medium can be expressed as

$$\nabla\cdot\mathbf{q}_R = \beta(1-\omega)(4n^2\sigma T^4 - G), \tag{6}$$

where β and ω denote the space-dependent extinction coefficient and single scattering albedo, respectively. The appropriate boundary conditions for the momentum and energy equations are

$$u = 0 \quad \text{for } r = R, 0 \leqslant z \leqslant L \tag{7a}$$

$$u = u_i \quad \text{for } r = r_i, 0 \leqslant z \leqslant L \tag{7b}$$

$$\left.\frac{\partial u}{\partial r}\right|_{r=r_i^+} = \left.\frac{\partial u}{\partial r}\right|_{r=r_i^-} \quad \text{for } r = r_i, 0 \leqslant z \leqslant L \tag{7c}$$

$$\frac{du}{dr} = 0 \quad \text{for } r = 0, 0 \leqslant z \leqslant L \tag{7d}$$

$$T = T_0 \quad \text{for } 0 \leqslant r \leqslant R, z = 0 \tag{8a}$$

$$T = T_w \quad \text{for } r = R, 0 \leqslant z \leqslant L \tag{8b}$$

$$T = T_i \quad \text{for } r = r_i, 0 \leqslant z \leqslant L \tag{8c}$$

$$k_f\left.\frac{\partial T}{\partial r}\right|_{r=r_i^+} = k_e\left.\frac{\partial T}{\partial r}\right|_{r=r_i^-} \quad \text{for } r = r_i, 0 \leqslant z \leqslant L \tag{8d}$$

$$\frac{dT}{dz} = 0 \quad \text{for } 0 \leqslant r \leqslant R, z = L. \tag{8e}$$

Selecting T_0 and R as the reference temperature and length, and defining the characteristic velocity as

$$u_c = \frac{R^2}{\mu}\left(-\frac{dp}{dz}\right)_{r_i=0} \tag{9}$$

one can write the nondimensional variables and parameters as follows:

$$\xi = r/R, \quad \eta = z/R \tag{10),(11}$$

$$\tilde{u} = u/u_c \quad \theta = T/T_0 \tag{12),(13}$$

$$\tilde{G} = G/4\sigma T_0^4 \quad \tilde{I} = I/4\sigma T_0^4 \tag{14),(15}$$

$$\tilde{q}_r = \frac{q_r}{k_f T_0/R} \quad \tilde{q}_x = \frac{q_x}{k_f T_0/R} \tag{16),(17}$$

$$\tau_f = \beta_f R \quad \tau_p = \beta_p R \tag{18),(19}$$

$$Pr = \frac{\nu}{k_f/\rho c_p} \quad Re = \frac{u_c R}{\nu} \tag{20),(21}$$

$$N = \frac{k_f/R}{4\sigma T_0^3} \quad \Gamma = \frac{\delta R F}{\sqrt{K}} \tag{22),(23}$$

$$\gamma = \frac{k_f}{k_e} \quad h = \frac{\sqrt{K}}{R} \tag{24),(25}$$

$$\Lambda = \left(\frac{dp}{dz}\right) \Big/ \left(\frac{dp}{dz}\right)_{r_i=0}. \tag{26}$$

In the dimensionless form, the governing equations, i.e. equations (1)–(4) and (6), are rewritten as

$$\frac{1}{\xi}\frac{d}{d\xi}\left(\xi\frac{d\tilde{u}}{d\xi}\right) = -\Lambda \tag{27}$$

$$RePr\tilde{u}\frac{\partial\theta}{\partial\eta} = \left[\frac{1}{\xi}\frac{\partial}{\partial\xi}\left(\xi\frac{\partial\theta}{\partial\xi}\right) + \frac{\partial^2\theta}{\partial\eta^2}\right] - \frac{\tau_f}{N} \tag{28}$$

$$\frac{1}{\xi}\frac{d}{d\xi}\left(\xi\frac{d\tilde{u}}{d\xi}\right) - \left(\frac{1}{h^2} + \Gamma Re\tilde{u}\right)\tilde{u} = -\Lambda \tag{29}$$

$$\gamma RePr\tilde{u}\frac{\partial\theta}{\partial\eta} = \left[\frac{1}{\xi}\frac{\partial}{\partial\xi}\left(\xi\frac{\partial\theta}{\partial\xi}\right) + \frac{\partial^2\theta}{\partial\eta^2}\right] - \frac{\tau_p}{N/\gamma}\Phi \tag{30}$$

$$\Phi = (1-\omega)(n^2\theta^4 - \tilde{G}). \tag{31}$$

Radiative transfer equation (RTE)

In the present study, radiation heat transfer is calculated using the newly developed S-type integral equation of transfer [11]. This method is preferred, because it can exactly calculate the radiation heat transfer in a two-dimensional, emitting, absorbing and isotropically scattering nonhomogeneous participating medium. For the reason stated above, it is believed that the results thus obtained are more accurate than those obtained by the S_N discrete coordinate or differential approximation methods. From the computational aspect, this method is also very efficient in handling combined heat transfer problems.

The incident radiation and two components of net radiative heat flux in the r- and z- directions are expressed as

$$\begin{pmatrix} \tilde{G}(\xi,\eta) \\ N\tilde{q}_r(\xi,\eta) \\ N\tilde{q}_z(\xi,\eta) \end{pmatrix} = 2\int_{\xi=0}^{1}\int_{\phi=0}^{\pi} \tilde{I}(\xi,\eta,\xi',\phi,0) \begin{pmatrix} \eta \\ \eta(\xi-\xi'\cos\phi)/d(\xi,\xi',\eta,\phi) \\ \eta^2/d(\xi,\xi',\eta,\phi) \end{pmatrix} \times \frac{\xi'\,d\xi'\,d\phi}{d^3(\xi,\xi',\eta,\phi)} + 2\int_{\xi'=0}^{1}\int_{\phi=0}^{\pi} \tilde{I}(\xi,\eta,\xi',\phi,\eta_L) \times \begin{pmatrix} \eta_L-\eta \\ (\eta_L-\eta)(\xi-\xi'\cos\phi)/d(\xi,\xi',\eta-\eta_L,\phi) \\ -(\eta_L-\eta)^2/d(\xi,\xi',\eta-\eta_L,\phi) \end{pmatrix} \times \frac{\xi'\,d\xi'\,d\phi}{d^3(\xi,\xi',\eta-\eta_L,\phi)} + 2\int_{\eta'=0}^{\eta_L}\int_{\phi=0}^{\pi} \tilde{I}(\xi,\eta,1,\phi,\eta') \times \begin{pmatrix} 1-\xi\cos\phi \\ (1-\xi\cos\phi)(\xi-\cos\phi)/d(\xi,1,\eta-\eta',\phi) \\ (\eta-\eta')(1-\xi\cos\xi)/d(\xi,1,\eta-\eta',\phi) \end{pmatrix} \times \frac{d\phi\,d\eta'}{d^3(\xi,1,\eta-\eta',\phi)} \quad \text{for } 0 \leqslant \xi \leqslant 1, \quad 0 < \eta < \eta_L, \tag{32), (33), (34)}$$

where the distance between a point (ξ',ϕ,η') on the boundary and a point $(\xi,0,\eta)$ in the flow region can be evaluated by

$$d(\xi,\xi',\eta-\eta',\phi) = \sqrt{\xi^2+(\xi')^2+(\eta-\eta')^2-2\xi\xi'\cos\phi}. \tag{35}$$

The formal solution of the intensity at $(\xi,0,\eta)$, which directs from (ξ',ϕ,η') to the point under consideration, is given by

$$\tilde{I}(\xi,\eta,\xi',\phi,\eta') = \tilde{I}_w(\xi',\eta')\exp[-\tau\,d(\xi,\xi',\eta-\eta',\phi)] + \int_{s=0}^{d(\xi,\xi',\eta-\eta',\phi)} \tilde{S}(\xi_s,\eta_s)\exp\{-\tau_s(\xi,\xi',\eta-\eta',\phi)\} \times \tau'(\xi',\eta')\,ds, \tag{36}$$

where $\tau'(\xi',\eta')$ is equal to either τ_f or τ_p, depending on whether the point (ξ',η') is within fluid layer or porous core. The source function is

$$\tilde{S}(\xi_s,\eta_s) = \frac{1}{4\pi}[(1-\omega)n^2\theta^4(\xi_s,\eta_s) + \omega\tilde{G}(\xi_s,\eta_s)]. \tag{37}$$

The formulations for the optical distances, τ and τ_s, are given in the Appendix. The position coordinates (ξ_s,η_s) are evaluated by

$$\xi_s(s) = \sqrt{(\xi')^2 - 2s\xi'\frac{\xi'-\xi\cos\phi}{d(\xi,\xi',\eta-\eta',\phi)} + s^2\frac{d^2(\xi,\xi',0,\phi)}{d^2(\xi,\xi',\eta-\eta',\phi)}} \tag{38a}$$

and

$$\eta_s(s) = \eta' + s\frac{\eta-\eta'}{d(\xi,\xi',\eta-\eta',\phi)}. \tag{38b}$$

The boundary conditions for the radiative transfer equation are the isotropical, external incident radiation from the free surface at the two ends (where $\eta = 0$ and η_L, respectively) and the diffuse cylindrical wall. The entering intensities from the three bounding surfaces can be specified by

$$\tilde{I}_w(\xi,0) = \theta^4(\xi,0)/4\pi \tag{39a}$$

$$\tilde{I}_w(\xi,\eta_L) = \theta^4(\xi,\eta_L)/4\pi \tag{39b}$$

$$\tilde{I}_w(1,\eta) = \frac{\varepsilon}{4\pi}\theta_w^4(\eta) + \frac{\rho^d}{\pi/N}\tilde{q}_{r,out}(1,\eta). \tag{39c}$$

It is noted that equations (32)–(34) are defined for all locations within the participating medium. The incident radiation and two components of net radiative heat flux on the three bounding surfaces are given as

$$\tilde{G}(\xi',\eta') = 2\pi I_w(\xi',\eta') + \tilde{G}_{out}(\xi',\eta')$$

$$\text{for } 0 \leqslant \xi' \leqslant 1, \eta' = 0 \text{ or } \eta_L \text{ and } \xi' = 1, 0 \leqslant \eta' < \eta_L \tag{40}$$

$$\tilde{q}_r(1,\eta') = -\pi I_w(1,\eta')/N + \tilde{q}_{r,out}(1,\eta') \quad \text{for } 0 \leqslant \eta' < \eta_L \tag{41}$$

$$\tilde{q}_z(\xi',\eta') = -\pi I_w(\xi',\eta')/N + \tilde{q}_{z,out}(\xi',\eta') \quad \text{for } 0 \leqslant \xi' < 1, \eta' = 0 \text{ or } \eta_L, \tag{42}$$

where $\tilde{G}_{out}(\xi',\eta')$, $\tilde{q}_{r,out}(1,\eta')$ and $\tilde{q}_{z,out}(\xi',\eta')$ are the incident radiation and normal component of heat fluxes irradiated from the medium onto the corresponding boundaries, respectively; their values can be calculated by substituting the proper coordinates (ξ',η') into equations (32)–(34).

Solution method

For the fluid layer (i.e. $\xi_i < \xi < 1$), the velocity distribution and velocity gradient at the interface are obtained by direct integration of equation (27), i.e.

$$\tilde{u}(\xi) = \frac{\Lambda}{4}(1-\xi^2) + \left(u(\xi_i) - \Lambda\frac{1-\xi_i^2}{4}\right)\frac{\ln\xi}{\ln\xi_i} \tag{43}$$

and

$$\tilde{u}(\xi_i) = \frac{\Lambda}{4}(1-\xi_i^2) + \left(\frac{\Lambda}{2}\xi_i + \left.\frac{d\tilde{u}}{d\xi}\right|_{\xi=\xi_i}\right)\xi_i \ln\xi_i, \tag{44}$$

while for the porous medium, the flow field is solved by applying an iterative scheme to the finite difference equation of equation (29) with the aid of analytical solutions of equations (43) and (44). Starting with an initial guess for the velocity profile and velocity gradient at the interface, an approximate velocity solution is obtained for two flow regions and then is used to improve the interface velocity gradient, with which a better velocity profile is obtained. The iteration continues until the velocity solution converges. It is found that an under-relaxation factor is required to ensure the convergence.

A grid size, 41 × 201 (radial × longitudinal), is selected for solving the energy equations of the fluid layer and porous core. Grid dependence has been checked by repeating the calculations with finer mesh sizes. Nearly identical results were obtained. Since it is found that solution of the S-type integral radiative transfer equation is rather insensitive to the grid size used [11], the number of nodes used for the radiation transfer is half of that used for the temperature field. For the intermediate points, the radiative quantities required for the solution of energy equation are obtained by linear interpolation. Using this approach the solutions obtained remained nearly unaffected, but the computational effort is greatly reduced. Same as the flow equations, the combined energy and radiative transfer equations are solved numerically by an iterative procedure. With the grid specified, the CPU time for a typical run on a CRAY C-90 supercomputer is about 2 h.

For evaluations of the combined convection–radiation heat transfer, the local Nusselt number is defined as

$$Nu(\eta) = 2\frac{\tilde{q}(1,\eta)}{\theta_m - \theta_w}, \tag{45}$$

where the mean bulk temperature, θ_m, is calculated by

$$\theta_m(\eta) = \frac{\int_0^1 \theta(\xi,\eta)\tilde{u}(\xi)\xi\,d\xi}{\int_0^1 \tilde{u}(\xi)\xi\,d\xi} \tag{46}$$

and the net heat flux, $\tilde{q}(1,\eta)$, transferred from the fluid to the heat-absorbing wall may be separated into two terms to take into account individual contribution from convection and radiation modes.

$$\tilde{q}(1,\eta) = -\frac{\partial\theta(1,\eta)}{\partial\xi} + \tilde{q}_r(1,\eta). \tag{47}$$

Thus, the local Nusselt number can be further expressed by

$$Nu(\eta) = Nu_C(\eta) + Nu_R(\eta), \tag{48}$$

where the contribution from convection is given by

$$Nu_C = \frac{2}{\theta_w - \theta_m}\frac{\partial\theta(1,\eta)}{\partial\xi} \tag{49}$$

and the contribution by radiation is

$$Nu_R = \frac{2}{\theta_m - \theta_w}\tilde{q}_r(1,\eta). \tag{50}$$

From the local Nusselt number, the averaged Nusselt number can be evaluated by

$$Nu_m(\eta) = \frac{1}{\eta_L}\int_0^{\eta_L} Nu(\eta)\,d\eta. \tag{51}$$

3. RESULTS AND DISCUSSION

In this study, the porous core is assumed to have a foam-type structure with a high porosity. In addition, the length of the duct is fixed at $L = 10R$ (or $\eta_L = 10$). The radiative properties and structural characteristics are taken from the available data in the literature [14, 15]. The representative values of the related non-dimensional parameters are: $\tau_p = 10$, $\omega_p = 0.75$, $\gamma = 0.3$, $h = 0.1$ and $\Gamma = 1.7$. For simplicity, it is assumed that the gas layer is nonscattering, and the optical thickness τ_f is specified as 0.0, 0.01 and 0.1 in the parametric analysis. The test runs show that the

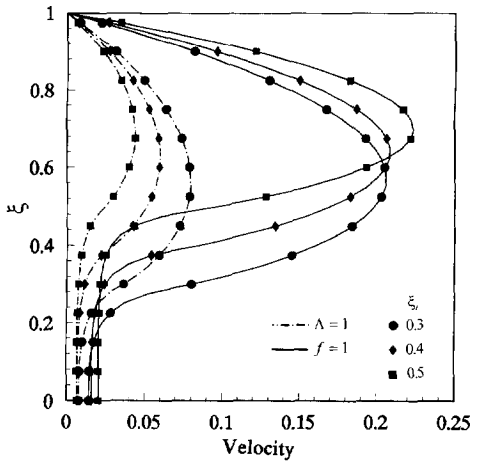

Fig. 2. Velocity distribution for $\xi_i = 0.3$, 0.4, 0.5; $\Gamma Re = 8500$.

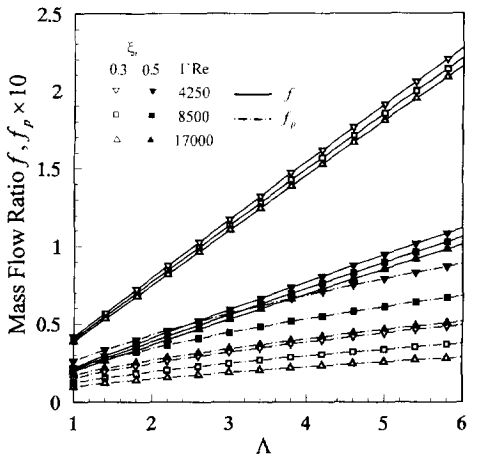

Fig. 3. Mass flow ratio as a function of the pressure gradient ratio, Λ, for $\xi_i = 0.3$, 0.5; $\Gamma Re = 4250$, 8500, 17 000.

numerical results are quite insensitive to the variations of the parameter τ_p, ω_p and γ.

Velocity profiles are shown in Fig. 2 for porous cores with various radius. For comparison, the velocity profiles are shown for two flow conditions; one is constant pressure gradient ($\Lambda = 1$) and the other a constant flow rate ($f = 1$). The mass flow ratio defined as $f = \dot{m}/\dot{m}_{i=0}$ is calculated by

$$f = 16 \int_0^1 \tilde{u}(\xi)\xi \, d\xi. \tag{52}$$

For the first case ($\Lambda = 1$), the pumping power is fixed and is the same as that without a porous core. Due to the increased flow resistance (proportional to the surface area of porous core), the mass flow rate is reduced as the radius of porous core is increased. On the other hand, if the mass flow rate is maintained constant ($f = 1$), it is observed that the maximum flow velocity is increased with the radius of the porous core. Of course, it is understood that the increase in the maximum flow velocity comes with the penalty of increased pressure drop, as will be elaborated later. However, for both cases, it can be seen that most fluid flows through the annular region confined by the porous core and bounding wall. Only a small portion of the mass flow moves in the core region, which is a direct consequence of the Darcy behavior of the porous medium. Due to the high porosity (relatively large h value), the inertial effect is appreciable near the outer region of the porous core. It is conceivable that this flow characteristic is beneficial for the increase of the convective heat transfer on the heat absorbing wall and in the fluid/porous core interface region.

The mass flow ratio, f, as depicted in Fig. 3, shows a linear dependence on the ratio of pressure gradient Λ. In contrast to the effect of parameter ΓRe, the porous core radius ξ_i shows a dominant role in determining the flow characteristics. When the ratio of pressure gradient is unity, the mass flow rate is reduced by 60–80% because of the presence of the porous core. To maintain the original mass flow rate, the required pumping power will be increased several times, as indicated in Table 1. The mass flow rate in the porous core, f_p, is smaller than the total flow rate by an order of magnitude for the cases considered.

The combined heat transfer enhancement using porous CRC may be illustrated by the isotherms for four different cases shown in Fig. 4. The radiation effect is neglected in cases (a) and (b), but is included in cases (c) and (d) in which the optical thickness of gas layer, τ_f, is specified as 0.0 (negligible gas radiation) and 0.1, respectively. With the insertion of the porous core while maintaining the same flow rate, the temperature gradient at the heat-absorbing wall is noticeably increased from case (a) to (b), due to the increase of the maximum flow velocity which results in a substantial heat transfer enhancement by convection. With the inclusion of radiative heat transfer in the energy equation, the isotherm in case (c) indicates that the porous core is rapidly cooled by self radiation, due to its strong radiative emittance and large surface per unit volume. At a relatively low temperature, the porous core also receives energy from the surrounding gas layer through convective transfer at the fluid/porous interface. Thus, a considerable amount of

Table 1. Effect of pressure gradient ratio, Λ, on the mass flow ratio f and f_p

ξ_i	Λ	f (%)	f_p (%)	ΓRe
0.3	1.0	34.0	1.2	8500
	2.7	103.0	2.3	8500
0.4	1.0	29.2	1.7	8500
	3.7	99.6	3.9	8500
0.5	1.0	20.4	2.1	8500
	5.3	99.8	8.2	4250
	5.6	99.5	6.5	8500
	6.0	101.3	5.2	17 000

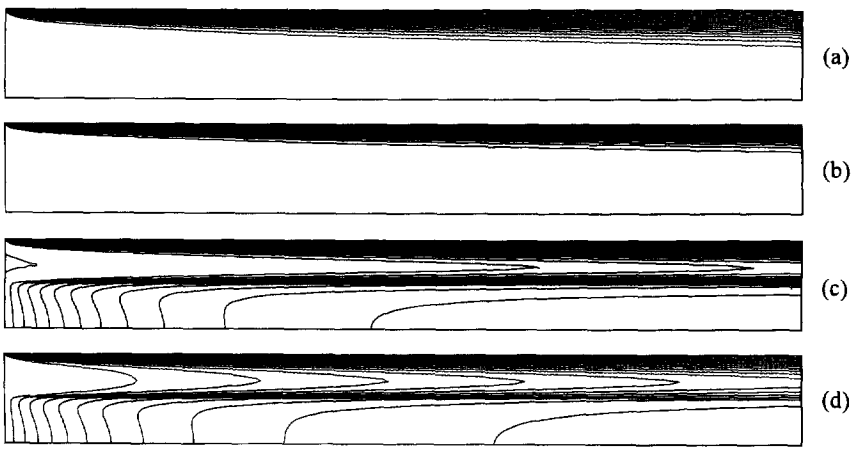

Fig. 4. Isotherms in four different flow systems: (a) $\xi_i = 0.0$ (no porous core); (b) $\xi_i = 0.5$ (pure convection); (c) $\xi_i = 0.5$, $\tau_f = 0.0$ (negligible gas radiation); and (d) $\xi_i = 0.5$, $\tau_f = 0.1$ (combined convection/radiation); $\Lambda = 5.6$; $\theta_w = 0.2$; N = 0.002 and $PrRe = 4000$.

energy carried by the fluid may be converted into radiative heat flux and emitted toward the heat-absorbing wall. For an optically thicker gas layer (gas is hotter than the core), case (d) shows that more heat transfer is obtained.

To assess the convective heat transfer augmentation, the local convection flux at the wall $q_C(1, \eta)$ is presented in Fig. 5 for the cases with $\xi_i = 0$ and 0.5. Given a mass flow rate (e.g. $f = 1$), the total convective heat flux is found to be increased by more than 40% using a porous core. Obviously, the increase is due to the significant alteration of the flow field. In the case of $\xi_i = 0.5$, about 93% of the fluid flows through the annular region, but only accounts for 75% of the total cross-sectional area. As the optical thickness of gas layer increases from zero to 0.1, the increased radiative heat transfer allows the gas medium to be cooled more effectively, which results in a reduction in the convective heat transfer rate.

It is noted that the heat transfer enhancement in radiation mode, as shown in Fig. 6, is most effective for the optically thin case. For a nonradiating gas layer (i.e. only wall and external incident radiation are considered), the porous core yields an augmentation in total radiative heat flux by 22% and a more uniform flux distribution is observed. The high radiation flux near the inlet is mainly due to the strong external incident radiation. A stronger emittance/absorptance of the gas layer tends to reduce the radiation enhancement of the porous core. When $\tau_f = 0.01$, the increase in radiative flux is found to be only 10% over the pure flow case, while for $\tau_f = 0.1$ the radiative flux is even further reduced.

Additional calculations show that the influences of scattering albedo and optical radius of the porous medium on the heat transfer rate are not significant. Because of high radiation dissipation, the porous core is cooled much faster than the gas layer along the flow direction. Thus, it is expected that if more fluid is allowed to flow into the porous core, the radiation

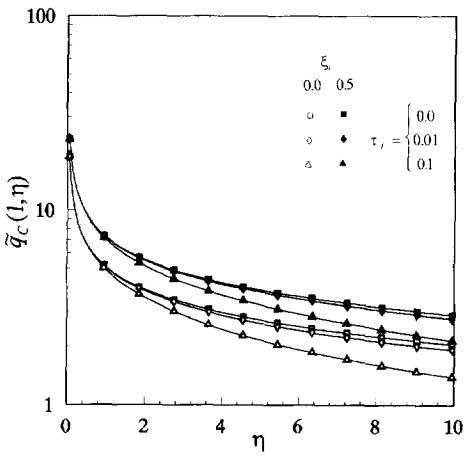

Fig. 5. Distributions of convective heat flux, $q_C(\eta)$, along the cylindrical wall for $\xi_i = 0.0, 0.5$; $\tau_f = 0.0, 0.01, 0.1$; $\Lambda = 5.6$; $\theta_w = 0.2$; N = 0.002 and $PrRe = 4000$.

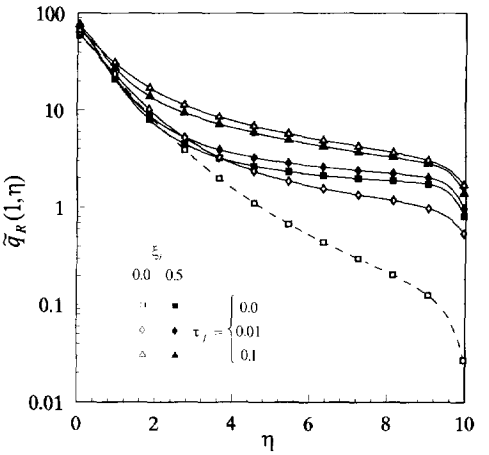

Fig. 6. Distributions of net radiative heat flux, $q_R(1, \eta)$, along the cylindrical wall for $\xi_i = 0.0$, 0.5; $\tau_f = 0.0$, 0.01, 0.1; $\Lambda = 5.6$; $\theta_w = 0.2$; N = 0.002 and $PrRe = 4000$.

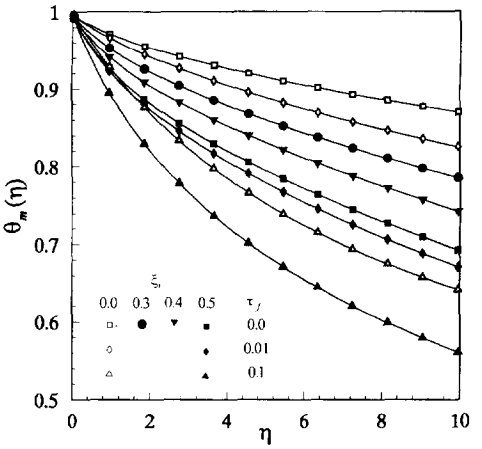

Fig. 7. Variation of mean temperature, $\theta_m(\eta)$, with longitudinal distance η for different radii, $\xi_i = 0.0, 0.3, 0.4, 0.5$; $f = 1.0$; $\tau_f = 0.0, 0.01, 0.1$; $\theta_w = 0.2$; $N = 0.002$ and $PrRe = 4000$.

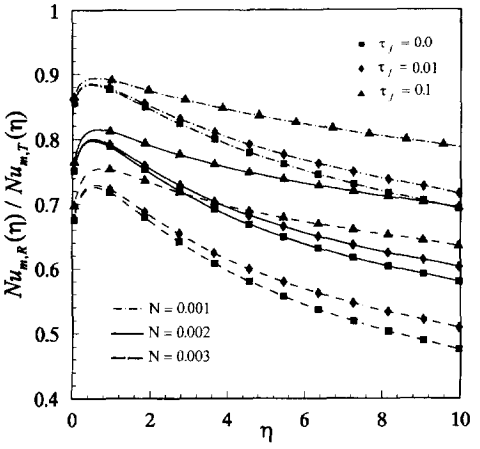

Fig. 9. Effect of conduction–radiation parameter on the ratio of modified radiative to total Nusselt number for radiation dominant cases, $\xi_i = 0.5$; $\Lambda = 5.6$; $\theta_w = 0.2$; $\tau_f = 0.0, 0.01, 0.1$; and $PrRe = 4000$.

heat transfer could be further enhanced. This can be accomplished by using CRC with a higher porosity and less flow resistance. For example, a porous annulus may be better than a porous core in terms of the pressure drop involved.

The mean bulk temperature profiles θ_m for different porous core radii and wall temperatures are plotted in Figs. 7 and 8. For the nonradiating gas case, the exit mean temperature is lowered from its original value of 0.87 to 0.79, 0.74 and 0.69 as the porous core radius ξ_i is increased from 0.3 to 0.4 and 0.5, respectively. Although the reduction in exit mean temperature is doubled as the porous core radius ξ_i is increased from 0.3 to 0.5, a two-fold pressure drop is required to maintain the same mass flow rate according to Fig. 3. However, as discussed earlier, the penalty arising from the increased pumping power can be minimized through the optimal design of the CRC structure. As the wall temperature increases, the heat transfer enhancement becomes less effective due to the stronger wall irradiation and reduced local radial temperature gradient.

In the flow system with a porous core, the radiative transfer mode is found to be dominant over the convection mode for $\eta > 0.5\eta_L$, where a strong radiation field is formed by the porous medium at a high temperature. The ratio of the averaged radiative Nusselt number to the total one, as plotted in Fig. 9, indicates that when the conduction–radiation parameter $N < 0.003$, most of the heat transport is by radiation mode, especially for a stronger radiating gas medium.

To illustrate the effect of Peclet number on the heat transfer, several comparative cases with and without a porous core are listed in Table 2 for $Pe = 2000$, 4000 and 8000. Apparently, the Peclet number has a significant influence on both the averaged convective and radiative Nusselt numbers when a porous core is present, while for the pure pipe flow the only noticeable effect is on the convective Nusselt number. This

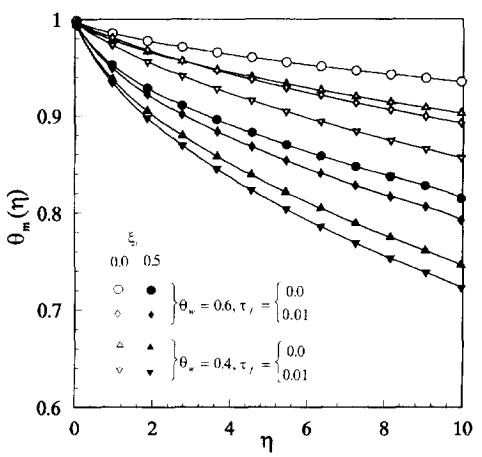

Fig. 8. Variation of room temperature, $\theta_m(\eta)$, with longitudinal distance η for $\xi_i = 0.0, 0.5$; $f = 1.0$; $\tau_f = 0.0, 0.01$; $N = 0.002$ and $PrRe = 4000$.

Table 2. Variations of modified convective and radiative Nusselt number and mean bulk temperature with $PrRe$, $\theta_w = 0.2$ and $N = 0.002$

ξ_i	$PrRe$	$Nu_{m,C}(\eta_L)$	$Nu_{m,R}(\eta_L)$	$\theta_m(\eta_L)$
			$\tau_f = 0.0$	
0.0	2000	7.26	15.67	0.80
	4000	8.99	15.31	0.87
	8000	11.29	15.10	0.92
0.5	2000	11.82	17.62	0.65
	4000	14.87	20.64	0.69
	8000	17.58	23.45	0.78
			$\tau_f = 0.01$	
0.0	2000	7.26	18.59	0.74
	4000	8.99	18.56	0.82
	8000	11.26	18.80	0.89
0.5	2000	13.10	21.16	0.53
	4000	14.89	22.73	0.67
	8000	17.58	25.99	0.77

is because the averaged radial temperature gradient at the wall and temperature in the outer porous core region are increased for a larger Peclet number, which leads to a stronger convection and radiation. As the Peclet number increases, the augmentation of heat transfer diminishes, and a smaller reduction in the exit mean temperature is found.

4. CONCLUSION

The enhancement of combined convective and radiative heat transfer using a porous core in a circular duct has been numerically investigated. An integral equation method is employed for the calculation of the radiation field in a two-layer nonhomogeneous participating medium. The highly nonlinear governing equations for the temperature and radiation fields are solved using an iterative scheme.

The numerical results show that the insertion of a porous core in a circular duct will not only increase the convective heat transfer, but also enhance the heat transport by radiation. It is found that the proposed system is particularly effective for a gas medium with a weak emittance, a slower velocity and a lower wall temperature (i.e. a smaller τ_f, Pe and θ_w). Although an increase in the porous core radius will lead to an increase in the heat transfer enhancement, it does have a penalty, in that the required pumping power also increases. Further heat transfer augmentation and power requirement reduction are possible if more fluid is directed through the porous core. This can be realized by optimizing the pore structure such that it has a higher porosity and less flow resistance. Also, the core geometry can be modified to have a hollow or partially hollow configuration. These possible improvements over the proposed system are currently under investigation.

Acknowledgements—This work was sponsored in part by US Department of Energy under contract DE-FG22-94BC 14971. The numerical calculations were performed on the supercomputer C-90. The supercomputer time provided by Cray Research Inc., administrated through Michael D. Tuttle, is gratefully acknowledged.

REFERENCES

1. R. Echigo, Effective energy conversion method between gas enthalpy and thermal radiation and application to industrial furnaces. In *Heat Transfer*-1982, Vol. 6, pp. 361–366. Hemisphere, Washington, DC (1982).
2. R. Echigo, M. Kurusu, K. Ichimiya and Y. Yoshizawa, Combustion augmentation of extremely low calorific gases, *Proceedings of the* 1983 *ASME/JSME Thermal Engineering Joint Conference*, Honolulu, Vol. 4, 99–103 (1983).
3. R. Echigo, High temperature heat transfer augmentation. In *High Temperature Heat Exchangers* (Edited by A. E. Sheidlin and N. Afghan), pp. 230–259. Hemisphere, Washington, DC (1986).
4. R. Echigo, Sophisticated applications of radiation heat transfer. In *Heat Transfer in High Technology and Power Engineering* (Edited by W.-J. Wang and Y. Mori), pp. 503–514. Hemisphere, Washington, DC (1987).
5. R. Echigo, H. Yoshida and T. Mochizuki, Temperature equalization by radiative converter for a slab in continuous casting-direct rolling, *Proceedings of the Second ASME/JSME Thermal Engineering Joint Conference*, Vol. 5, pp. 63–69 (1987).
6. R. Echigo, K. Hanamura, Y. Yoshizawa and T. Tomimura, Radiative heat transfer enhancement to a water tube by combustion gases in porous media. In *Heat Transfer Science and Technology* (Edited by B.-X. Wang), pp. 703–710. Hemisphere, Washington, DC (1987).
7. K. Y. Wang and C. L. Tien, Thermal insulation in flow systems: combined radiation and convection through a porous segment, *J. Heat Transfer* **106,** 453–459 (1984).
8. R. Echigo, Y. Tomimura, Y. Yoshizawa and H. Innouchi, Effective energy conversion method between gas enthalpy and thermal radiation (effects of gaseous radiation and incoming radiation), Report of Institute of Advanced Material Study, Kyusyu University, Vol. 2, pp. 53–66 (1988).
9. H. Yoshida, J. H. Yun and R. Echigo, Transient characteristics of combined conduction, convection and radiation heat transfer in porous media, *Int. J. Heat Mass Transfer* **33,** 847–857 (1990).
10. T. W. Tong, M. C. Sharatchandra and Z. Gdoura, Using porous inserts to enhance heat transfer in laminar fully-developed flows, *Int. Commun. Heat Mass Transfer* **20,** 761–770 (1993).
11. J. M. Zhang and W. H. Sutton, Predictions of radiative transfer in two-dimensional nonhomogeneous participating cylindrical media, *J. Thermophys. Heat Transfer* **10,** 47–53 (1996).
12. K. Kamiuto, M. Sato and M. Iwamoto, Determination of the radiative properties of high-porosity materials by use of the emerging-intensity fitting method, *J. Quant. Spectrosc. Radiat. Transfer* **42,** 477–482 (1989).
13. R. Mital, J. P. Gore and R. Viskanta, Measurements of extinction coefficient and single scattering albedo of reticulated porous ceramic at high temperatures, *The Thirtieth AIAA Thermophysics Conference*, AIAA paper 95-2036 (1995).
14. M. Kaviany, *Principles of Heat Transfer in Porous Media*. Springer, New York (1991).

APPENDIX

The optical distance τ and τ_s in equation (36) are determined according to the path a radiation beam travels through. For the porous core region where $0 \leqslant \xi \leqslant \xi_i$, we have

(a) $\xi' \leqslant \xi_i$ and $\eta' = 0$ or $\eta' = \eta_L$

$$\tau(\xi, \xi', \eta - \eta', \phi) = \tau_p \, d(\xi, \xi', \eta - \eta', \phi) \tag{A1}$$

$$\tau_s(\xi, \xi', \eta - \eta', \phi) = \tau_p[d(\xi, \xi', \eta - \eta', \phi) - s] \quad \text{for } 0 \leqslant s \leqslant d(\xi, \xi', \eta - \eta', \phi); \tag{A2}$$

(b) $\xi_i < \xi' \leqslant 1$ and $0 \leqslant \eta' \leqslant \eta_L$

$$\tau(\xi, \xi', \eta - \eta', \phi) = \tau_f x_f + \tau_p x_p, \tag{A3a}$$

where

$$x_p = \frac{d(\xi, \xi', \eta - \eta', \phi)}{d(\xi, \xi', 0, \phi)} \left\{ \frac{\xi(\xi - \xi' \cos\phi)}{d(\xi, \xi', 0, \phi)} + \sqrt{\left[\frac{\xi(\xi - \xi' \cos\phi)}{d(\xi, \xi', 0, \gamma)} \right]^2 - \xi^2 + \xi_i^2} \right\} \tag{A3b}$$

$$x_f = d(\xi, \xi', \eta - \eta', \phi) - x_p \tag{A3c}$$

$$\tau_s(\xi,\xi',\eta-\eta',\phi)=\tau_f(x_f-s)+\tau_p x_p \quad \text{for } 0\leqslant s\leqslant x_f \tag{A4a}$$

$$\tau_s(\xi,\xi',\eta-\eta',\phi)=\tau_p[d(\xi,\xi',\eta-\eta',\phi)-s]$$
$$\text{for } x_f\leqslant s\leqslant d(\xi,\xi',\eta-\eta',\phi). \tag{A4b}$$

For the fluid layer where $\xi_i<\xi\leqslant 1$, we have

(a) $\xi'\leqslant\xi_i$ and $\eta'=0$ or η_L

$$\tau(\xi,\xi',\eta-\eta',\phi)=\tau_f x_f+\tau_p x_p, \tag{A5a}$$

where

$$x_p=\frac{d(\xi,\xi',\eta-\eta',\phi)}{d(\xi,\xi',0,\phi)}\left\{\frac{\xi'(\xi'-\xi\cos\phi)}{d(\xi,\xi',0,\phi)}\right.$$
$$\left.+\sqrt{\left[\frac{\xi'(\xi'-\xi\cos\phi)}{d(\xi,\xi',0,\phi)}\right]^2-(\xi')^2+\xi_i^2}\right\} \tag{A5b}$$

$$x_f=d(\xi,\xi',\eta-\eta',\phi)-x_p \tag{A5c}$$

$$\tau_s(\xi,\xi',\eta-\eta',\phi)=\tau_p(x_p-s)+\tau_f x_f \quad \text{for } 0\leqslant s\leqslant x_p \tag{A6a}$$

$$\tau_s(\xi,\xi',\eta-\eta',\phi)=\tau_f[d(\xi,\xi',\eta-\eta',\phi)-s]$$
$$\text{for } x_p\leqslant s\leqslant d(\xi,\xi',\eta-\eta',\phi); \tag{A6b}$$

(b) $\xi_i<\xi'\leqslant 1$, $0\leqslant\eta'\leqslant\eta_L$ and $0\leqslant\phi\leqslant\cos^{-1}\xi_i/\xi+\cos^{-1}\xi_i/\xi'$

$$\tau(\xi,\xi',\eta-\eta',\phi)=\tau_f\, d(\xi,\xi',\eta-\eta',\phi) \tag{A7}$$

$$\tau_s(\xi,\xi',\eta-\eta',\phi)=\tau_f[d(\xi,\xi',\eta-\eta',\phi)-s]; \tag{A8}$$

(c) $\xi_i<\xi'\leqslant 1$, $0\leqslant\eta'\leqslant\eta_L$ and $\cos^{-1}\xi_i/\xi+\cos^{-1}\xi_i/\xi'<\phi\leqslant\pi$

$$\tau(\xi,\xi',\eta-\eta',\phi)=\tau_f(x_{f1}+x_{f2})+\tau_p x_p, \tag{A9a}$$

where

$$x_{f1}=\frac{d(\xi,\xi',\eta-\eta',\phi)}{d(\xi,\xi',0,\phi)}[\sqrt{(\xi')^2-h^2}-\sqrt{\xi_i^2-h^2}] \tag{A9b}$$

$$x_{f2}=\frac{d(\xi,\xi',\eta-\eta',\phi)}{d(\xi,\xi',0,\phi)}[\sqrt{\xi^2-h^2}-\sqrt{\xi_i^2-h^2}] \tag{A9c}$$

$$x_p=d(\xi,\xi',\eta-\eta',\phi)-x_{f1}-x_{f2} \tag{A9d}$$

and

$$h=\frac{\xi\xi'}{d(\xi,\xi',0,\phi)}\sin(\pi-\phi) \tag{A9e}$$

$$\tau_s(\xi,\xi',\eta-\eta',\phi)=\tau_f(x_{f1}-s+x_{f2})+\tau_p x_p \quad \text{for } 0\leqslant s\leqslant x_{f1} \tag{A10a}$$

$$\tau_s(\xi,\xi',\eta-\eta',\phi)=\tau_f x_{f2}+\tau_p(x_{f1}+x_p-s)$$
$$\text{for } x_{f1}\leqslant s\leqslant x_{f1}+x_p \tag{A10b}$$

$$\tau_s(\xi,\xi',\eta-\eta',\phi)=\tau_f[d(\xi,\xi',\eta-\eta',\phi)-s]$$
$$\text{for } x_{f1}+x_p\leqslant s\leqslant d(\xi,\xi',\eta-\eta',\phi). \tag{A10c}$$